A Kalman Filtering Approach to Multispectral Image Classification and Detection of Changes in Signature Abundance

Chein-I Chang, *Senior Member, IEEE*, and Clark M. Brumbley

***Abstract*—Subpixel detection and classification are important in identification and quantification of multicomponent mixtures in remotely sensed data, such as multispectral/hyperspectral images. A recently proposed orthogonal subspace projection (OSP) has shown some success in Airborne Visible/Infrared Imaging Spectrometer (AVIRIS) and Hyperspectral Digital Imagery Collection Experiment (HYDICE) data. However, like most techniques, OSP has its own constraints. One inherent limitation is that the number of signatures to be classified cannot be greater than that of spectral bands. Owing to this limitation, OSP may not perform well for multispectral imagery as it does for hyperspectral imagery. This phenomenon is observed by three-band Satellite Pour l'Observation de la Terra (SPOT) data because of an insufficient number of spectral bands compared to the number of materials to be classified. Further, most approaches proposed for multispectral and hyperspectral image analysis, including OSP, operate on a pixel by pixel basis. In this case, a general assumption is made on the fact that the image data are stationary and pixel independent. Unfortunately, this may be true for laboratory data, but not for real data, due to varying atmospheric and scattering effects. In this paper, a Kalman filtering approach is presented that overcomes the aforementioned problems. In addition to the observation process described by a linear mixture model, a Kalman filter utilizes an abundance state equation to model the nonstationary nature in signature abundance. As a result, the signature abundance can be estimated and updated recursively by the Kalman filter and an abrupt change in signature abundance can be detected via the abundance state equation. The effectiveness of the proposed Kalman filtering approach is demonstrated through computer simulations and SPOT data. The experimental results show the potential of the proposed Kalman filtering-based approach in multispectral image analysis.**

***Index Terms*—Classification, detection, estimation, hyperspectral image, Kalman filter, Kalman filter-based linear mixing (KFLM), multispectral image, orthogonal subspace projection (OSP).**

I. Introduction

SUBSPACE projection is a versatile technique that has been commonly used in signal processing and neural networks for a wide range of applications, such as data compression, dimensionality reduction, and pattern recognition. Most recently, it also found an application in remote sensing [1], in which an orthogonal subspace projection (OSP) classifier was developed for hyperspectral image classification and showed some success in Airborne Visible/Infrared Imaging Spectrometer (AVIRIS) data. One of the important applications in multispectral and hyperspectral imaging is target detection and image classification. However, due to the nature of image acquisition, an image pixel is generally mixed by various materials present in that pixel. As a result, many image processing techniques cannot be directly applied and need to be modified. OSP takes advantage of subspace projection so as to achieve dimensionality reduction and feature extraction. Since OSP was introduced, it has been successfully applied to Hyperspectral Digital Imagery Collection Experiment (HYDICE) images [2]. Nevertheless, like most techniques, OSP can be improved by relaxing assumptions, such as *a priori* knowledge about signatures. Along this line, some efforts [3]–[4] have been made to enhance and extend the capability of OSP to adapt to unknown environments. A class of OSP-based methods were reported to show the potential and usefulness of OSP in HYDICE data exploitation [4]. For example, several *a posteriori* versions of OSP were proposed to estimate signature abundance in [5] and an adaptive OSP-based technique, called constraint energy minimization (CEM) [6], was also presented for classification with unknown signatures and background. However, there is an inherent limitation on OSP that cannot be relaxed. It is called the band number constraint (BNC), which is that the number of signatures to be classified should not be greater than that of spectral bands. When OSP is developed for hyperspectral images, BNC never becomes an issue because the number of signatures of interest is generally far less than that of spectral bands, such as 224-band AVIRIS data and 210-band HYDICE data. Unfortunately, if OSP was applied to multispectral imagery, it was found that OSP could not effectively reject undesired signatures due to a small number of bands used to collect data containing a large number of signature classes.

In order to see why, let U and $\langle U \rangle$ be the set of undesired signatures and the space linearly spanned by U, respectively. We also let $\langle U \rangle^{\perp}$ denote the subspace orthogonal to $\langle U \rangle$. As OSP is applied, it first employs a subspace annihilator denoted by $P_U^{\perp}$ to reject undesired signatures in U by projecting the observed pixel into $\langle U \rangle^{\perp}$ so that the effects of undesired signatures can be eliminated. Since the hyperspectral images, such as AVIRIS and HYDICE images, are acquired by more

Manuscript received August 4, 1997; revised February 17, 1998.

C.-I Chang is with the Remote Sensing Signal and Image Processing Laboratory, Department of Computer Science and Electrical Engineering, University of Maryland Baltimore County, Baltimore, MD 21250 USA (e-mail: cchang@umbc2.umbc.edu).

C. M. Brumbley is with the United States Department of Defense, Fort Meade, MD USA.

Publisher Item Identifier S 0196-2892(99)00040-6.

than 200 spectral bands that are generally greater than signatures to be classified, the rejection of undesired signatures can be properly done in a space with large dimensionality. However, this may not be true for multispectral imagery with the total number of used bands less than the number of signatures. In this case, not all undesired signatures in U can be rejected by $P_U^{\perp}$ because the dimensionality of the rejection space is smaller than that of $\langle U\rangle^{\perp}$. As a result, some undesired signatures in U may be mixed into $\langle U\rangle^{\perp}$ and will garble the desired signature. This scrambled desired signature further deteriorates the performance of the matched filter, which follows the projector $P_U^{\perp}$ in the OSP approach. Consequently, the overall classification performance of OSP is degraded. In this paper, this phenomenon is demonstrated by Satellite Pour l'Observation de la Terra (SPOT) data.

By realizing that the BNC is a constraint directly resulting from subspace projection, we need to reinvent an approach other than subspace projection to cope with this dilemma. In this paper, we present a Kalman filter-based linear mixing approach, called KFLM, to relax the BNC. In addition to the linear mixture model used by OSP, KFLM employs an auxiliary equation, called abundance state equation (ASE), to trace the signature abundance. In other words, KFLM adopts the linear mixture model to represent the admixture of pixels while utilizing an ASE to keep track of changes in signature abundance. Several prominent advantages can be gained by including the ASE in KFLM. One is to allow us to detect an abrupt change from pixel to pixel in a nonstationary background. Another is to provide us with the information about the spatial correlation between pixels. More importantly, the inherent constraint BNC imposed on OSP does not exist in KFLM since KFLM is designed independent of data projection that is used in the OSP approach. It provides a new means to look at the mixed pixel classification problems besides subspace projection. Although Kalman filtering is not a new concept, applying the Kalman filtering to linear mixing problems in multispectral/hyperspectral image classification seems to be a new application. As shown in experiments conducted in this paper, KFLM not only performs better than OSP in three-band SPOT data, in which the BNC is imposed, but also is comparable to OSP in hyperspectral image classification, in which case the BNC is not an issue [7]. In order to make OSP still applicable to multispectral image analysis, a remedy is suggested.

The organization of this paper is given as follows. Section II describes a linear mixing problem and KFLM approach, in which two Kalman filtering equations are introduced to model multispectral image pixels and signature abundance. Section III presents computer simulations to show the capability of the KFLM in detecting abrupt change in signature abundance and SPOT data experiments to show the constraint of OSP. A comparative study is also made between KFLM and OSP methods, and OSP is amended for multispectral image applications. Section IV draws a brief conclusion.

II. KFLM for Mixed Pixel Classification

A. Linear Mixing Problems

One of widely used techniques in multispectral/hyperspectral image classification is linear unmixing, which uses a linear mixture model to unmix the components in the mixture. More precisely, assume that l is the number of spectral bands and p is the number of signature vectors. Let $\boldsymbol{r}(x,y)$ be an $l\times 1$ column vector, and denote the image pixel at the location (x,y). Next, define an $l\times p$ signature matrix S as $S=(\boldsymbol{s}_1\boldsymbol{s}_2\cdots\boldsymbol{s}_p)$, where $\boldsymbol{s}_j$ is an $l\times 1$ column vector representing the spectral signature of the jth material. Finally, define an $l\times 1$ abundance vector $\alpha(x,y)$ denoted by $\alpha(x,y)=(\alpha_1(x,y)\alpha_2(x,y)\cdots\alpha_p(x,y))^T$, where $\alpha_j(x,y)$ represents the abundance of the jth material in the pixel at location (x,y). The linear mixture model is then given by

$$\boldsymbol{r}(x,y)=S\alpha(x,y)+\boldsymbol{v}(x,y) \tag{1}$$

where the signature matrix S is assumed to be invariant to spatial location and the $l\times 1$ vector $\boldsymbol{v}(x,y)$ represents white additive noise with zero mean and covariance matrix, given by $\sigma_1^2 I_{l\times l}$, with $I_{l\times l}$ being the $l\times l$ identity matrix. Equation (1) is a widely used linear mixture model from which many linear unmixing methods can be derived.

B. Motivation

The motivation of developing KFLM arises from an attempt to improve and enhance the OSP approach so as to adapt itself to more challenging environments, such as unknown noise, unknown signatures, unknown background and interference, etc. As mentioned in Section I, several OSP-based methods were developed to extend OSP capability in detecting a low-probability target in unknown background, such as LPD in [6], or in an adaptive means, such as CEM in [6], or in *a posteriori* fashion by taking advantage of observation information to estimate the signature abundance, such as *a posteriori* LSOSP in [4], or in an unsupervised manner to estimate unknown signatures from the background, such as UODSP in [8]. However, all of these methods are bound to the subspace projection with an inherent limitation, the BNC. As a consequence, they may not be suitable for multispectral image analysis. As shown in [4], *a posteriori* LSOSP can significantly improve OSP performance if the background noise is known *a priori*. Unfortunately, it is not often the case for real data. One way to mitigate this problem is to use an adequate statistical model to describe the noise. Inspired by the work in [4], it prompts us to look into the potential of the Kalman filtering in hyperspectral image applications in which the measurement equation in conjunction with the state equation can be used to model the noise resident in pixels and the noise in signature abundance. A few immediate advantages can result from the Kalman filtering, as follows.

1) Kalman filtering is recursive and a well-known real-time processing technique widely used in control, communication, and signal processing communities. This implies that a technique designed based on Kalman filtering should be practical in real applications.
2) It can be used to process nonstationary data. This is an important advantage over OSP for processing remotely sensed image data due to unknown parameters and atmospheric and scatter effects.

3) It is adaptive and updates the abundance state by taking into account the interpixel spatial correlation. Compared to OSP, which works on a pixel by pixel basis, a Kalman filtering-based technique provides more information than OSP. Consequently, it should perform better than OSP if models are chosen properly.
4) There is no BNC in KFLM. This advantage makes KFLM applicable to applications in multispectral images.

It should be noted that, despite the success of the Kalman filtering in many fields, there still remains some challenging problems, such as the model selection and parameter estimation.

C. KFLM Approach

The KFLM presented in this subsection is a Kalman filter with the linear mixture model given by (1) as the measurement equation and state equation given by the following abundance equation:

$$\alpha(k+1) = \Phi(k+1,k)\alpha(k) + \boldsymbol{u}(k) \tag{2}$$

where the spatial position (x, y) in (1) is replaced by k to indicate the discrete time instant k at which the pixel is currently being processed. The vector $\alpha(k)$ represents the amount of the abundance at time k, and $\Phi(k+1, k)$ is a known $p \times p$ state transition matrix used to describe the state of the change in the abundance from time k to time $k+1$. $\boldsymbol{u}(k)$ is the $p \times 1$ abundance noise vector independent of $\alpha(k)$ and assumed to be a zero-mean, white process with covariance matrix given by

$$E[\boldsymbol{u}(k)\boldsymbol{u}(m)^T] = Q = \sigma_2^2 \delta_{km} I_{p\times p} \tag{3}$$

where σ_2^2 is the variance of the abundance noise vector, δ_{km} is Kronecker's notation given by

$$\delta_{km} = \begin{cases} 1, & k = m \\ 0, & k \neq m \end{cases}$$

and the matrix $I_{p\times p}$ represents the $p \times p$ identity matrix. In accordance with the discrete-time Kalman filtering notation at discrete time k, we rewrite (1) as

$$\boldsymbol{r}(k) = S(k)\alpha(k) + \boldsymbol{v}(k) \tag{4}$$

where the vector $\boldsymbol{r}(k)$ represents the observed pixel at time k and $S(k)$ is a known signature matrix at time k. The measurement noise is represented by $\boldsymbol{v}(k)$ in (1), which is assumed to be a zero-mean, white process with covariance matrix given by

$$E[\boldsymbol{v}(k)\boldsymbol{v}(m)^T] = R = \sigma_1^2 I_{l\times l}\delta_{km}. \tag{5}$$

The goal of KFLM is to obtain the minimum mean-squared estimate of the abundance state $\alpha(k)$ given that the data $\boldsymbol{r}(k)$ are observed. Using the knowledge of the predicted $\alpha(k)$, we can classify and detect the pixel $\boldsymbol{r}(k)$.

Let $\hat{\alpha}(k+1|k)$ represent the minimum mean-squared predictor of $\alpha(k+1)$ given the past observations $\boldsymbol{r}(j)$ for all j from one to k. $\hat{\alpha}(k|k), \hat{\alpha}(k|k-1)$ are also defined similarly. We further define $P(k|k)$ to be the error covariance matrix at time k given the past observations $\boldsymbol{r}(j)$ for all j from one to k and $P(k+1|k)$ to be the one-step prediction error covariance matrix at time $k+1$ given the past observations $\boldsymbol{r}(j)$ for all j from one to k. Then KFLM is performed recursively as follows. For detailed implementation of Kalman filtering, refer to [9].

- *Initial Conditions*:
  R and Q
  $\hat{\alpha}(0|-1)$: mean of $[\alpha(0)] = E[\alpha(0)]$;
  $P(0|-1)$: covariance matrix of $[\alpha(0) = \mathrm{Cov}[\alpha(0)]$.
- *Kalman Gain*: Compute Kalman gain at the current time k

$$K(k) = [\Phi(k+1,k)P(k|k-1)S^T(k)] \\ [S(k)P(k|k-1)S^T(k) + R(k)]^{-1}. \tag{6}$$

- *Abundance and Error Measurement Updates*:
  a) Update the abundance estimate at the current time k with $\boldsymbol{r}(k)$

$$\hat{\alpha}(k|k) = \hat{\alpha}(k|k-1) + K(k)[\boldsymbol{r}(k) - S(k)\hat{\alpha}(k|k-1)]. \tag{7}$$

  b) Update the error covariance matrix at the current time k

$$P(k|k) = [I - K(k)S(k)]P(k|k-1). \tag{8}$$

- *Abundance and Error Measurement Predictions*:
  a) Predict the abundance at next time $k+1$

$$\hat{\alpha}(k+1|k) = \Phi(k+1,k)\hat{\alpha}(k|k). \tag{9}$$

  b) Predict the error covariance matrix at next time $k+1$

$$P(k+1|k) = \Phi(k+1,k)P(k|k)\Phi^T(k+1,k) + Q. \tag{10}$$

D. Discussions

It should be noted that OSP and KFLM are developed based on different design rationales, even though they both share a linear mixture model. The former applies a subspace projection to pack the desired signature in a small subspace while rejecting undesired signatures so as to achieve dimensionality reduction and noise suppression. It does not require image statistics *a priori* nor the background noise. The latter takes a statistical approach, in which the measurement equation and ASE are described by statistical models. So, the performance of KFLM depends heavily on how accurately these two Kalman filtering equations fit the data, particularly, the model selection and parameter estimation of the ASE. This is a difficult and challenging problem in spectral estimation. In general, three statistical models can be used for this purpose, viz., moving average (MA), autoregressive model (AR), and autoregressive-moving average model (ARMA). Since investigating this problem is beyond the scope of the paper, it will not be discussed here. However, we will briefly describe a model to be used in this paper that is governed by a first-order Gauss–Markov process.

According to the ASE given by (2), we immediately recognize that it is indeed a first-order Gauss–Markov model that can be also viewed as a first-order AR model. The utilization

of the transition matrix $\Phi(k+1,k)$ is to describe the correlation between signatures from examining a pixel at time k to the next pixel at time $k+1$. In this paper, we assume that $\Phi(k+1,k)$ is an identity matrix. This means that the jth abundance $\alpha_j(k+1)$ at time $k+1$ is predicted solely on the abundance $\alpha_j(k)$ of its immediate past pixel. This type of prediction is generally referred to as the zero-order holder interpolation used in predictive coding, such as differential pulse code modulation (DPCM) in communications, signal, and image processing. Of course, we can replace the first-order Gauss–Markov model with a pth order AR by including more past pixels to improve prediction. However, in this case, we need to determine the model order p and the prediction coefficients. This problem has been studied extensively in array processing and spectral estimation [10]–[12]. Some criteria have been proposed for this purpose, such as an information criterion (AIC) [13] or minimum description length (MDL) [14].

III. Computer Simulations and SPOT Data Experiments

OSP has demonstrated its potential in hyperspectral image data for image classification and detection [1]–[6]. As mentioned previously, the application of OSP to multispectral imaging has not yet been explored. In this section, we will show that OSP does not perform well in real multispectral data as expected since the number of distinct undesired spectral signatures may be greater than the total number of spectral signatures, as shown in the following for three-band SPOT data in which there are more than three classes of materials to be discriminated. In this case, it is obvious that we cannot properly project more than two undesired signatures into a subspace with two dimensions (note that the desired signature space requires at least one dimension). Consequently, some undesired signatures will be blended into the desired signature that results in signal deterioration; a similar finding was also observed in [5].

In this section, we will demonstrate this phenomenon and show that KFLM outperforms OSP in both computer simulations and SPOT data, in which the ASE is modeled by a first-order Gauss–Markov process with the identity state transition matrix $\Phi(k+1,k)$.

A. Computer Simulations

A set of four spectral radiances directly extracted from a SPOT scene will be used in computer simulations to evaluate the performance of KFLM and OSP.

Experiment 1 (Mixed Pixel Classification): The spectral signatures used in the simulated data were obtained directly by extracting pixels from an image scene shown in Fig. 1. These data were collected by the SPOT system from three bands, two of which are from the visible region of the electromagnetic spectrum referred to as band 1 (0.50–0.59 μm) and band 2 (0.61–0.68 μm), and the third band is from the near-infrared region of electromagnetic spectrum referred to as band 3 (0.79–0.89 μm). These three images were coregistered and combined into an image cube. In this case, the term pixel refers to a 3×1 vector in which the three components of the vector correspond to the three bands of the SPOT data.

In order to generate desired signatures, four sets of pixels were extracted from four different scenes in the SPOT image that represent buildings, roads, vegetation, and water, respectively. Each set consists of nine pixels corresponding to a particular scene to be used for classification. For example, the building signature was generated from Falls Church High School, Falls Church, VA, the road signature from the Little River Turnpike, the water signature from the lake in the upper right of the image, and the vegetation signature from Mill Creek Park. All nine sample pixels were averaged and normalized, then used as the desired spectral signature of the materials they represent. These signatures shown in Fig. 2 were used to generate the 3×4 signature matrix S, in which the unit vectors were the columns of the matrix. This matrix was then used in (1) to generate the linearly mixed pixels that were used in the experiments. Since the SPOT image has only three dimensions, in order for OSP to work well on (1), no more than three signatures are allowed. In this case, four choices are possible. In the following experiment, we simply selected buildings, roads, and vegetation for desired signatures and set the water signature to 0%. Another three possibilities were also conducted, and their results were very similar to what we present here.

The first simulation was performed to determine the responses of KFLM and OSP to constant abundance levels of the materials. The 550 mixed pixels were generated using the three spectral signatures described above. The three signatures were combined in the abundance values given in Table I. White Gaussian noise was added to each pixel to generate signal-to-noise ratios (SNR's) of 30 : 1, in which the SNR was defined in [1] as 50% of the reflectance divided by the standard deviation of the noise.

The results of the simulations are given in Fig. 3, which shows the responses of KFLM and OSP operating on the simulated data. As seen in the figure, OSP did accurately estimate the abundance of any of the three materials. An observation about OSP can be made from the results in Fig. 3. That is, each operator had different scales for the minimum energy and the maximum energy. This occurs because OSP first projects the input pixel onto a space that is orthogonal to the undesired signatures. The space that the input pixel is projected onto changes for each desired signature. This projection is not done to maximize the energy within the desired signature, but to minimize the energy in the interfering undesired signatures. The result is that OSP can be used to determine if one pixel has more material of a desired signal than another pixel, but it cannot be used to determine if a single pixel has more material of one signature than another signature.

The results in Fig. 3 also show that KFLM accurately estimated the abundance of all three materials. This experiment demonstrates the strength of KFLM in estimating the abundance of multispectral data. The results also indicate that the estimate of KFLM for the abundance vector can track the abundances of different materials. As a consequence, KFLM can be used to determine if there is more abundance of one of the materials in the pixel than the other materials, while OSP performs neither of these functions.

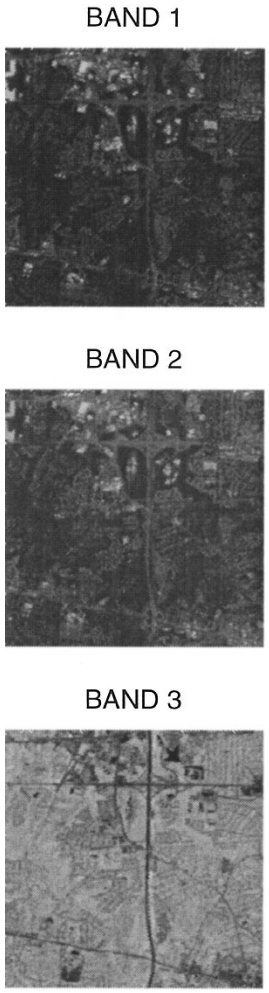

Fig. 1. Scene from SPOT data.

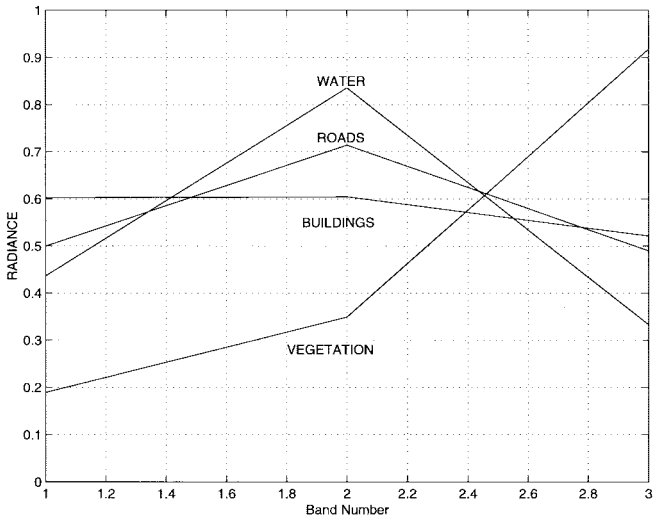

Fig. 2. Four radiances—buildings, roads, water, and vegetation—from SPOT data.

Experiment 2 (Detection of Abrupt Change in Abundance): The second experiment was performed to determine the responses of KFLM and OSP to abrupt changes in the abundance of the materials. This experiment addresses the fact that KFLM uses the abundance vector of the previous pixel to estimate the abundance vector of the current pixel being processed. This experiment was designed to see if large differences between the initial estimate and actual values of the abundance vector will have an affect on the estimate KFLM. Since OSP processes each pixel individually and independently, the estimate of the abundance is not applicable to OSP. The three spectral signatures employed in **Experiment 1** were used in this experiment. The three signatures were combined to form 550 mixed pixels with the abundance of the building signature equal to 0%, the abundances of the road signature and the water signature equal to 50%. Every fiftieth pixel of this sequence was replaced with a pixel that contains a nonzero abundance of the building signature and the remaining abundance split evenly between the road signature and the vegetation signature. The amount of the building signature in the fiftieth pixels started at 10% for the fiftieth, 20% for the hundredth, and so on, until the building signature abundance in the five hundredth pixel was 100%. White Gaussian noise was added to each pixel to generate SNR of 30 : 1. This experiment allows for observation of the response of KFLM to changes in abundance for only one pixel.

TABLE I
ABUNDANCE ASSIGNMENT FOR 550 SIMULATED PIXELS

Pixel	Building	Road	Vegetation
0-50	0.00	0.50	0.50
51-100	0.10	0.45	0.45
101-150	0.20	0.40	0.40
151-200	0.30	0.35	0.35
201-250	0.40	0.30	0.30
251-300	0.50	0.25	0.25
301-350	0.60	0.20	0.20
351-400	0.70	0.15	0.15
401-450	0.80	0.10	0.10
451-500	0.90	0.05	0.05
501-550	1.00	0.00	0.00

The results are shown in Fig. 4, which represents the output of KFLM corresponding to the abundance of the building signature in the pixel. Fig. 4 indicates that the estimate of the abundance generated by KFLM made an increase in the abundance of building signature at every fiftieth pixel. These abrupt increases were witnessed by the increase in values corresponding to the increasing abundance of building signature in the pixel. These results verify that a rapid change in the abundance vector between consecutive pixels can be accurately estimated by KFLM. Fig. 4 also shows the output of OSP corresponding to the three materials in which OSP could detect the occurrence of sudden changes, but the results of abundance estimate for each operator were based on different scales.

B. SPOT Experiments

In the following SPOT data experiments, we will demonstrate two things. One is the constraint BNC imposed on OSP. When it is violated, OSP performs poorly. On the other hand, KFLM does not have such limitation and still performs well. Another is an amendment of OSP that is modified for

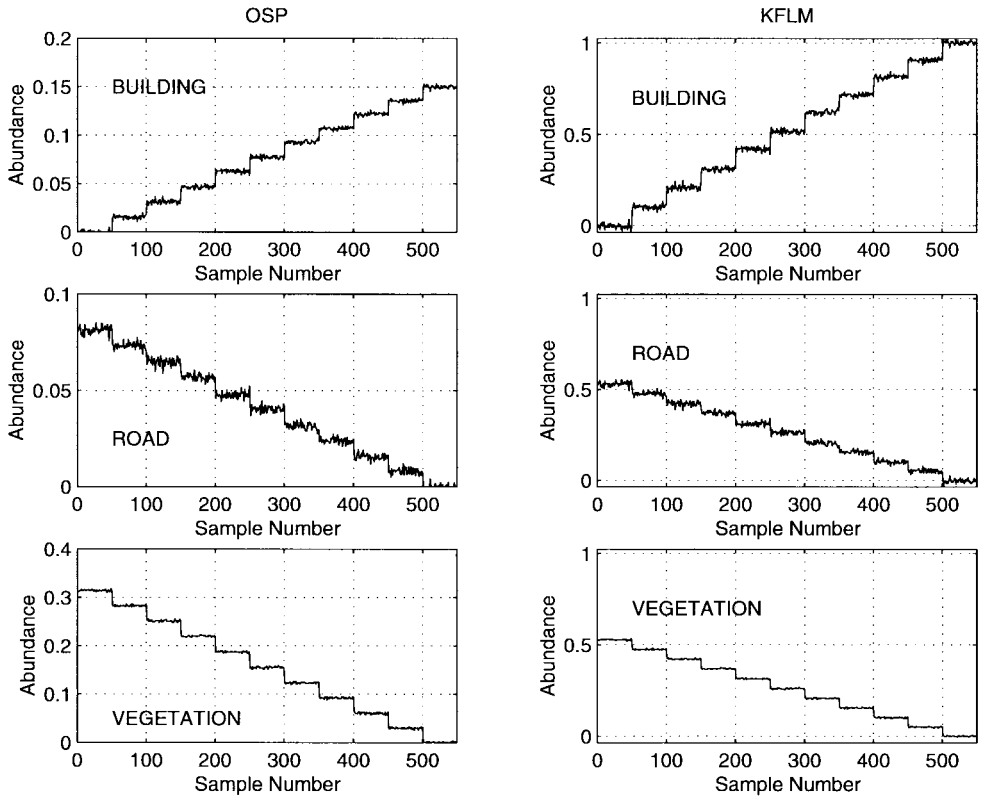

Fig. 3. Computer simulations for signature estimation.

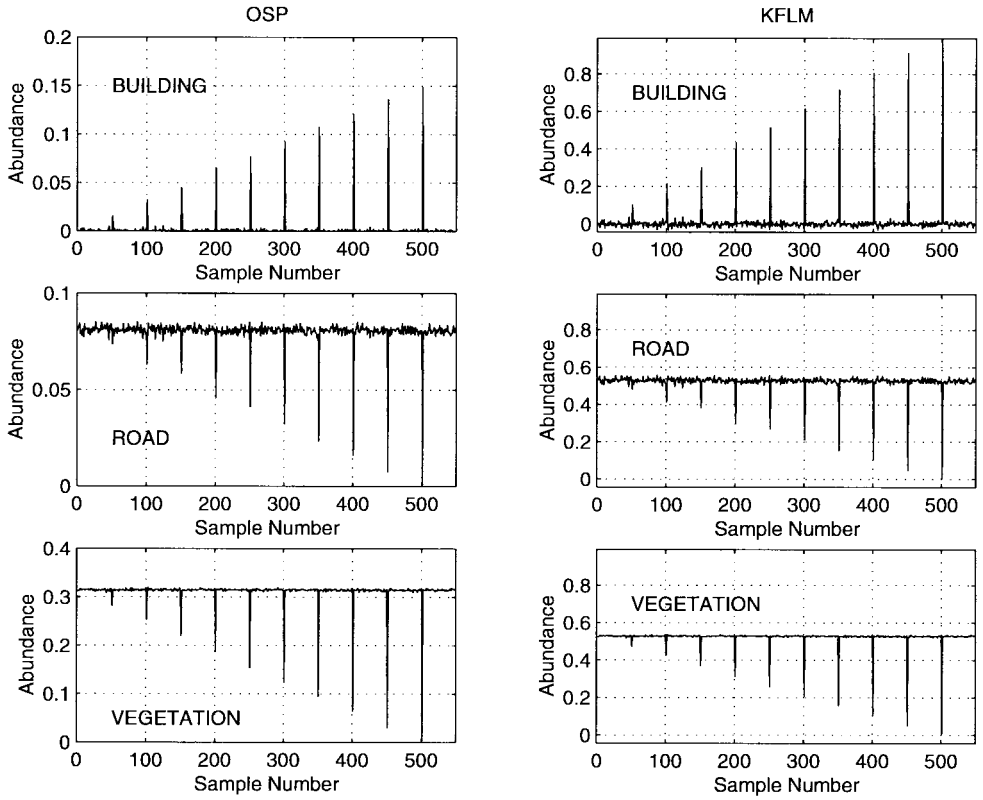

Fig. 4. Computer simulations for detection of abrupt change in abundance.

experiments. Even in this case, KFLM still outperforms OSP. The initial conditions to be used for SPOT data experiments were chosen empirically. The measurement noise R was chosen to achieve the ratio of the signature energy to noise energy, 20 dB, and for $\sigma_2^2 = 10\,000$ for $Q, \hat{\alpha}(0|-1) = 0$ and $P(0|-1) = 0$.

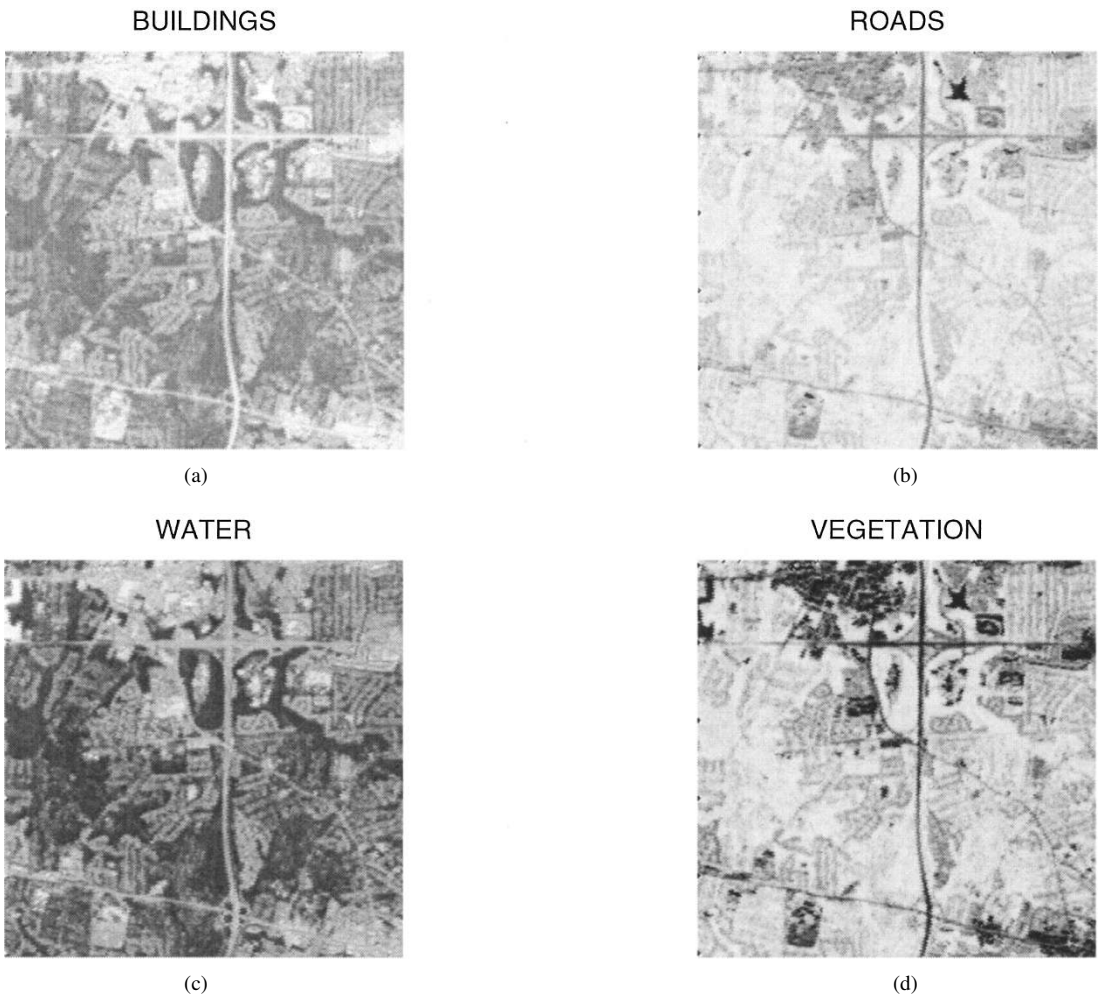

Fig. 5. SPOT experiments for OSP.

The scene in Fig. 1 contains several buildings, bodies of water, highways, and secondary roads. These features were used as desired signatures for KFLM and OSP. The signatures used were the same as the ones described previously in Section III-A. The three images in Fig. 1 are coregistered and have a ground sampling resolution of 20 m. The data used in this experiment are 256 $\times$ 256 pixels with 256 grayscales and thus represent 5120 $\times$ 5120 m. The pixel vectors were then normalized to create a unit vector before they were processed. These normalized pixel vectors were processed by KFLM and OSP.

1) OSP Results: OSP classifiers were generated for each of the four spectral signatures and then applied to the SPOT data. The results are provided in Fig. 5 compared to a map of the region given by Fig. 6. These four images are labeled according to the desired signature used to generate OSP classifiers. The images in Fig. 5 show that OSP fails to classify the targets of interest. The OSP classifier with the building signature as the desired signature shows the buildings in the scene. The OSP classifier with the desired signature for the water detected the buildings in the scene, but not the water. The OSP classifier with the roads signature as the desired signature did pick up the roads, but it also picked up the large lake in the area around the pixel at vertical position 175 and horizontal position 25. OSP classifier with the vegetation signature as the desired signature brings out the lake and the roads in the scene as the brightest areas. These four images show that the four OSP classifiers failed to locate pixels within the SPOT data that contained the desired signatures.

2) KFLM Results: Fig. 7 shows the SPOT results of the estimated abundance using KFLM and contains four images, building, roads, bodies of water, and vegetation, in the scene.

1) Fig. 7(a) shows that the areas where there were high levels of the abundance of the building signature correspond to buildings on the map. The Falls Church High School located in the area around the pixel at vertical position of 200, horizontal position of 75, and the Fairfax Hospital located in the area around the pixel at vertical position of 100, horizontal position of 100, appear as large white areas in the image. The region located in the area around the pixel at vertical position of 100, horizontal position of 25, contains several buildings in which individual buildings can be determined. Fig. 7(a) clearly shows the building located in the region.
2) Fig. 7(b) shows the results of KFLM estimating the abundance using the spectral signature of roads. The areas in the image that represent roads correspond to the location of roads on the map. The estimate of the

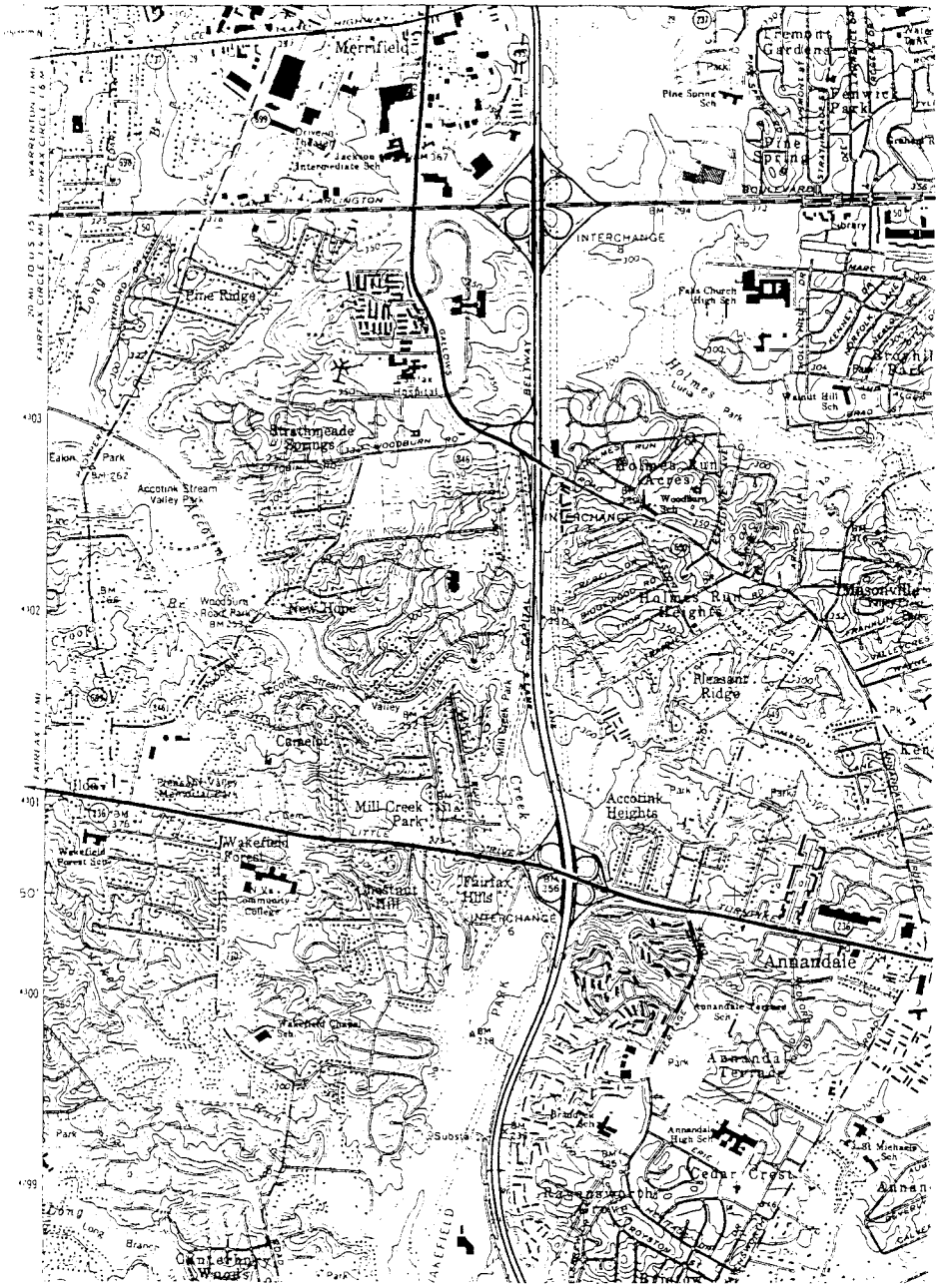

Fig. 6. Map of a scene from SPOT data.

abundance generated by KFLM not only revealed the major highways, but also the secondary and residential streets in the region. Even the turns and cul-de-sacs of the residential streets can be seen in this image. This can be seen most clearly in the area around the pixel at vertical position of 160 and horizontal position of 110. This area of the image shows a unique pattern of turns in the residential roads that could be seen in the corresponding area of the map. The results of the experiment also reveal large areas of roads near the top and bottom of the image. These large areas of roads occur around buildings and represent parking lots. Since parking lots were not represented on the map, a visit to the area was made to determine if these areas contained parking lots. The visit confirmed that these areas were parking lots. This evidence further proves that KFLM effectively and accurately estimates the position of the roads and parking lots in the region.

3) Fig. 7(c) shows the abundance estimate results generated by KFLM using the spectral signature of water. This image clearly indicates the lake located in the area around the pixel at a vertical position of 175 and horizontal position of 25. In addition, a small pond is also picked up in the area around the pixel at vertical position of 70 and horizontal position of 220, which can be identified in the map. Fig. 7(c) also shows that KFLM accurately estimates the position of the bodies of water in the region.

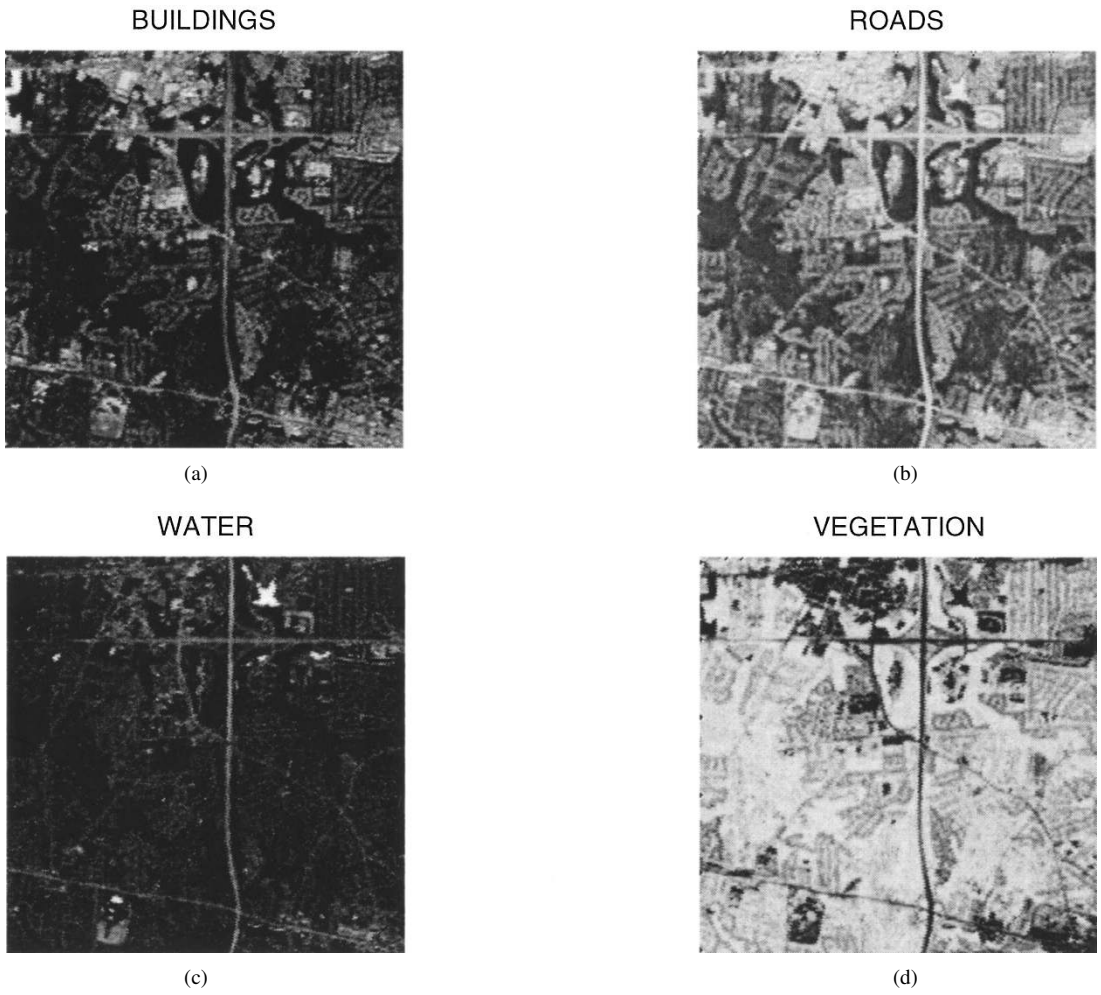

Fig. 7. SPOT experiments for KFLM. (a) Buildings as the desired signature. (b) Roads as the desired signature. (c) Water as the desired signature. (d) Vegetation as the desired signature.

4) Fig. 7(d) is the abundance results produced by KFLM using the spectral signature of vegetation. This image shows large areas of high levels of vegetation in almost all areas of the region. The map reveals many parks in the region. These parks include Accotink Stream Valley Park, Mill Creek Park, Wakefield Park, and Luria Park. The comparison of this image with the map confirms that the large areas of high levels of vegetation correspond to the parks and residential areas in the region. These are areas where high levels of vegetation should be expected. The dark areas in the images represent low levels of vegetation that correspond to areas where buildings, roads, parking lots, or bodies of water were located in the previous images. These are areas where no vegetation should be found.

The images discussed in Fig. 7(a)–(d) demonstrate that KFLM successfully classifies four different classes of materials, while OSP works poorly in classification.

3) Remedy for OSP: As demonstrated in Section III-B1, the performance of OSP was poor in classifying one desired signatures from three undesired signatures. This results from the BNC. In order to comply with this constraint, only two undesired signatures should be used in OSP. Under this circumstance, the remaining unused signature will be viewed as an interfering signature. So, three OSP operators can be generated from selecting two out of three undesired spectral signatures. These operators were then applied to the SPOT data in four different cases, each case corresponds to one interference selected from the four signatures, roads, buildings, water, and vegetation. The results showed that the KFLM performs better than OSP for all four cases. In this paper, only one selected for best illustration is shown in Fig. 8.

The images in Fig. 8 are the results of the three OSP operators with the road signature as the desired signature, two of three other signatures as undesired signatures, and the fourth as an interfering signature. The image in Fig. 8(a) is the result of OSP with the building and the water signature as undesired signatures and vegetation as interfering signatures. OSP could not detect the roads in the image. Instead, OSP detected the vegetation in the scene and appeared similar to the images generated by OSP with vegetation as the desired signature. When we applied OSP to the road and vegetation signatures, respectively, it was found that OSP detected almost ten times as much of the energy of the vegetation signature as for the road signature. The reason for this is that OSP projects the pixel's energy into a subspace orthogonal to

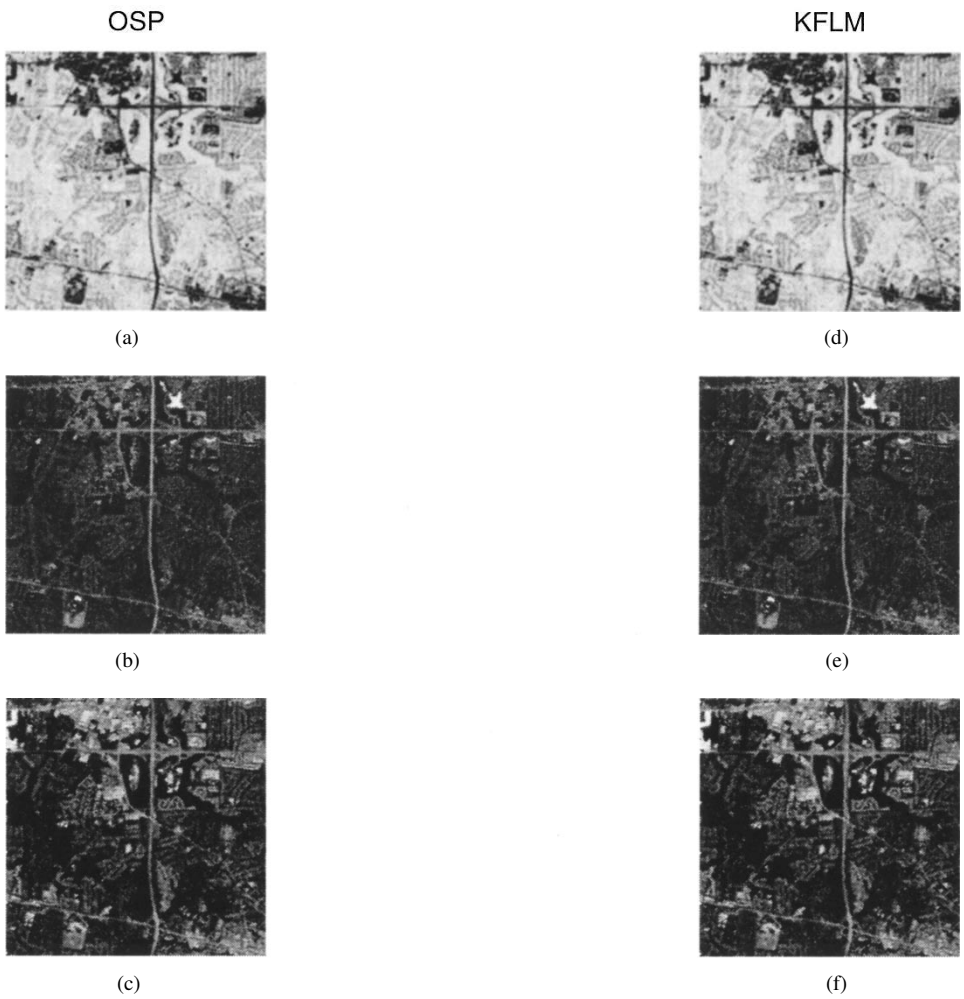

Fig. 8. OSP results using roads as the desired signature. (a) Buildings and water as undesired signatures and vegetation as an interfering signature. (b) Buildings and vegetation as undesired signatures and water as an interfering signature. (c) Vegetation and water as undesired signatures and buildings as an interfering signature. KFLM results using roads as the desired signature. (d) Buildings and water as undesired signatures and vegetation as an interfering signature. (e) Buildings and vegetation as undesired signatures and water as an interfering signature. (f) Vegetation and water as undesired signatures and buildings as an interfering signature.

the undesired signatures. This orthogonal subspace is close to being orthogonal to the desired signature if one of the undesired signatures is very similar to the desired signature. In this case, the signature for roads is very similar to the signature for water; hence, much of the energy from the road signature is eliminated by the projection. Fig. 8(b) is the result of OSP with the building and the vegetation signature as undesired signatures and the water as an interfering signature. OSP could detect the roads in the image, but it also could detect the lake in the scene. Again, applying OSP to the road and water signatures, respectively, showed that OSP detected twice as much of the energy of the water signature as for the road signature. These two images show that OSP has problems distinguishing between the similar signatures of roads and water. Fig. 8(c) is the result of OSP with the water and the vegetation signature as undesired signatures and the buildings as an interfering signature. The buildings in the scene can be seen more clearly in this image then the roads. Once again, applying OSP to the road and building signatures, respectively, shows that OSP detected twice as much of the energy of the buildings signature as for the road signature. These three images show very different results for the three OSP operators to detect roads. We also applied KFLM in comparison with OSP to the SPOT image scene in the same fashion as we did for Fig. 8(a)–(c), and the results are shown in Fig. 8(d)–(f), respectively. As we can see, KFLM performs better than does OSP. The same experiments were also conducted using buildings, water, and vegetation as desired signatures, respectively, and similar results were obtained but not included in this paper. The reason to select Fig. 8 for illustration is because roads and water have very similar signatures. This allows us to see how the undesired signature water interferes with the desired signature roads.

The above experiments showed that the performance of OSP depends on the relationship between the signatures. For instance, OSP using the road as desired signature with different combinations of undesired signatures has a significant effect on the performance of these operators. The water signature was so similar to the road signature that, if the water signature was not included as an undesired signature, OSP could not distinguish between the two classes. The OSP operator that included the water signature as an undesired

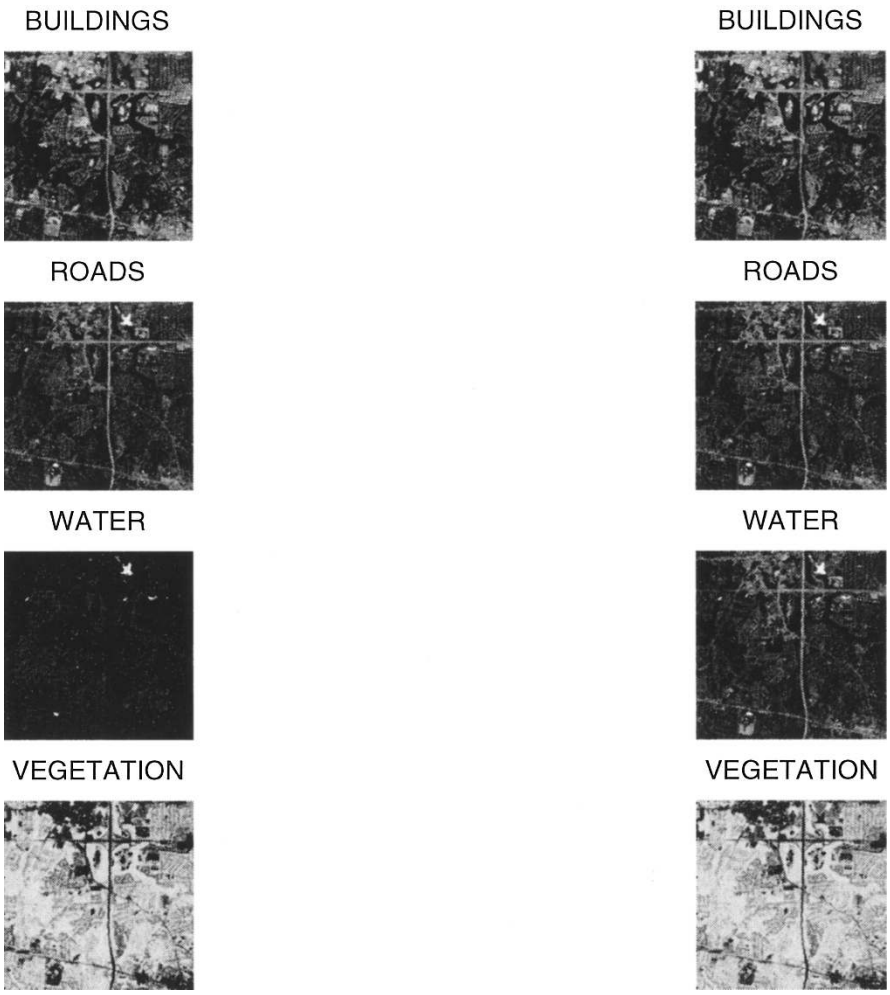

Fig. 9. Best four-class classification results generated by OSP (left column) and KFLM (right column), respectively.

signature reduced a significant amount of the road's energy while nulling out the water's energy. Since this operator annihilated so much of the road's energy, the energy from the interfering signature overwhelmed the OSP detector such that the operator mistakenly detected this interfering road signature. So, in order to implement OSP in multispectral imagery, a knowledge of the relationship between the target signatures is required to produce best results. The images in the left column of Fig. 9 show a set of best results in four-class (building, road, water, and vegetation) classification, which are selected from four different experiments. However, they do not come from the same OSP operator. This implies that one single OSP will not perform well when the number of undesired signatures is larger than the number of bands. In this case, a judicious selection of undesired signatures and interfering signature is necessary to warrant the applicability of OSP.

In order to compare the performance of KFLM against OSP, we applied the same signatures that were used for OSP to KFLM. A best four-class classification result is also selected and shown in the right column of Fig. 9. As expected, KFLM performed better than OSP.

IV. Conclusion

OSP has shown to be a promising technique in AVIRIS and HYDICE data analysis and exploitation. It was found that a constraint inherited from subspace projection prevents it from applications in multispectral image analysis. In this paper, we presented KFLM as an alternative to OSP, which can be used in multispectral and hyperspectral image analysis to detect and estimate nonstationary or pixel-varying signature abundance. The idea is to introduce an ASE into the linear mixture model so that the changes in abundance from pixel to pixel can be detected via the ASE. Since the two Kalman filter equations (i.e., linear mixture equation and abundance state equation) can be implemented recursively, the proposed KFLM has a potential in real-time data processing. The experimental results showed that KFLM not only performed better than OSP in computer simulations, but also worked effectively in SPOT data, of which OSP seemed to fail in classification. This failure is primarily attributed to the fact that a complete rejection of undesired signatures is not possible since it does not have a sufficient number of bands to accommodate the number of materials to be classified. On the other hand, KFLM does not have this constraint. With the help of the ASE, KFLM can further capture the nature of nonstationarity in real data and keep track of changes in signature abundance so as to achieve subpixel detection. Nevertheless, we do not claim that KFLM is a better technique than OSP in all aspects because they are completely different approaches and have different

strengths. For instance, OSP is particularly useful when there is no prior statistical knowledge available about the background, as demonstrated in [6] and [8], while KFLM will do better if the used models faithfully reflect the data. Finally, it should be noted that, in this paper, we only dealt with multispectral image classification problems. The same conclusion does not automatically apply to hyperspectral image classification in which the BNC is no longer a constraint. In this case, OSP and KFLM were shown in [7] to perform equally well in classification.

ACKNOWLEDGMENT

The authors would like to thank Dr. S.-Y. Hsu with Susquehanna Resources and Environment, Inc., for providing the SPOT data used in the experiments conducted in this paper.

REFERENCES

[1] J. Harsanyi and C.-I Chang, "Hyperspectral image classification and dimensionality reduction: An orthogonal subspace projection approach," *IEEE Trans. Geosci. Remote Sensing*, vol. 32, pp. 779–785, May 1994.
[2] *DARPA Spectral Exploitation Workshop*, Inf. Syst. Office Defense Adv. Res. Projects Agency, July 1–2, 1996, Annapolis, MD.
[3] *Spectroradiometric Working Group*, Interagency Training Center, VA, Feb. 3–4, 1997.
[4] T.-M. Tu, C.-H. Chen, and C.-I Chang, "A posteriori least squares orthogonal subspace projection approach to desired signature extraction and detection," *IEEE Trans. Geosci. Remote Sensing*, vol. 35, pp. 127–139, Jan. 1997.
[5] C.-I Chang, X. Zhao, M. L. G. Althouse, "Least squares subspace projection approach to mixed pixel classification for hyperspectral images," *IEEE Trans. Geosci. Remote Sensing*, vol. 36, pp. 898–912, May 1998.
[6] J. Harsanyi, *Detection and Classification of Subpixel Spectral Signatures in Hyperspectral Image Sequences*, Ph.D. dissertation, Dept. Elect. Eng., Univ. Maryland Baltimore County, Baltimore, MD, Aug. 1993.
[7] C. Brumbley and C.-I Chang, "A Kalman filtering approach to hyperspectral image classification," in *Proc. Conf. Inf. Sci. Syst.*, The Johns Hopkins Univ., Baltimore, MD, Mar. 19–21, 1997, pp. 179–184.
[8] C.-I Chang and C. Brumbley, "An orthogonization target signature space projection to image classification," in *Proc. Conf. Inf. Sci. Syst.*, The Johns Hopkins Univ., Baltimore, MD, Mar. 19–21, 1997, pp. 174–178.
[9] S. Haykin, *Adaptive Filtering Theory*, 3rd ed. Englewood Cliffs, NJ: Prentice-Hall, 1996.
[10] ———, *Advances in Spectrum Analysis and Array Processing*, vol. I. Englewood Cliffs, NJ: Prentice-Hall, 1991.
[11] ——— *Advances in Spectrum Analysis and Array Processing*, vol. II. Englewood Cliffs, NJ: Prentice-Hall, 1991.
[12] ———, *Advances in Spectrum Analysis and Array Processing*, vol. III. Englewood Cliffs, NJ: Prentice-Hall, 1995.
[13] N. Wax and T. Kailath, "Detection of signals by information theoretic criteria," *IEEE Trans. Acoust., Speech, Signal Processing*, vol. ASSP-33, pp. 1190–1197, Nov. 1985.
[14] J. Rissanen, "Modeling by shortest data description," *Automatica*, vol. 14, pp. 465–471, 1978.

Chein-I Chang (S'81–M'82–SM'92) received the B.S. degree from Soochow University, Taipei, Taiwan, R.O.C., in 1973, the M.S. degree from National Tsing Hua University, Hsinchu, Taiwan, in 1975, the M.A. degree from the State University of New York at Stony Brook in 1977, respectively, all in mathematics. He also received the M.S. and M.S.E.E. degrees from the University of Illinois, Urbana-Champaign, in 1980 and 1982, respectively, and the Ph.D. in electrical engineering from the University of Maryland, College Park, in 1987.

He was a Visiting Assistant Professor from January 1987 to August 1987, Assistant Professor from 1987 to 1993, and is currently Associate Professor in the Department of Computer Science and Electrical Engineering, University of Maryland Baltimore County. He was a Visiting Specialist in the Institute of Information Engineering, at National Cheng Kung University, Tainan, Taiwan, from 1994 to 1995. His research interests include information theory and coding, signal detection and estimation, multispectral/hyperspectral image processing, neural networks, and pattern recognition.

Dr. Chang is a member of SPIE, INNS, Phi Kappa Phi, and Eta Kappa Nu.

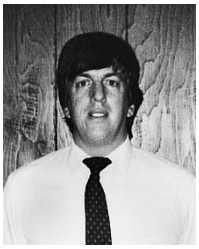

Clark M. Brumbley was born in Salisbury, MD, on April 15, 1961. He received the B.S.E.E. degree from Old Dominion University, Norfolk, VA, in 1985, the M.S.E.E and the Ph.D. degrees from the University of Maryland Baltimore County in 1993 and 1998, respectively.

He is a Senior Electronic Engineer with the United States Department of Defense, Fort Meade, MD. His research interests include signal detection and estimation and multispectral/hyperspectral image processing.

Dr. Brumbley is a member of Tau Beta Pi, Eta Kappa Nu, and Sigma Xi.